


Recent Advances in Nanoengineering of Electrode-Electrolyte Interfaces to Realize High-Performance Li-Ion Batteries

Na-Yeong Kim, Ilgyu Kim, Behnoosh Bornamehr, Volker Presser*, Hiroyuki Ueda, Ho-Jin Lee, Jun Young Cheong* , and Ji-Won Jung*

A suitable interface between the electrode and electrolyte is crucial in achieving highly stable electrochemical performance for Li-ion batteries, as facile ionic transport is required. Intriguing research and development have recently been conducted to form a stable interface between the electrode and electrolyte. Therefore, it is essential to investigate emerging knowledge and contextualize it. The nanoengineering of the electrode-electrolyte interface has been actively researched at the electrode/electrolyte and interphase levels. This review presents and summarizes some recent advances aimed at nanoengineering approaches to build a more stable electrode-electrolyte interface and assess the impact of each approach adopted. Furthermore, future perspectives on the feasibility and practicality of each approach will also be reviewed in detail. Finally, this review aids in projecting a more sustainable research pathway for a nanoengineered interphase design between electrode and electrolyte, which is pivotal for high-performance, thermally stable Li-ion batteries.

1. Introduction


Since their initial commercialization by Sony in the 1990s, lithium-ion batteries (LIBs) have attracted significant attention and are utilized in various applications, ranging from portable electronics to electric vehicles.^[1–5] The impact of the LIB was also honored by the selection of the 2019 Nobel Prize in Chemistry^[6] and has become one of the most successful recent technologies in our daily lives. The interface and interphase between the electrode and electrolyte have been critical factors in the past and current LIBs since they affect the performance, from cycle retention to rate capability.^[7–10] It is indispensable to have a stable electrode/electrolyte interface at both cathode^[11] and anode^[12] since Li⁺ ions reversibly move between the anode and cathode, and an unstable interface in either of the electrodes is detrimental to the electro-

chemical performance of LIBs.

Various factors affect the quality of the interface and interphase between electrode and electrolyte.^[13–15] For instance, various additives in the electrolyte greatly affect the interphase between the electrode and electrolyte,^[16,17] as even a minute change in the types of chemicals used in the electrolyte leads to the formation of interphase with varied composition. There is also a difference between liquid and gel/solid-state electrolytes (SSEs),^[18] where the formed interface between the electrode and electrolyte shows distinct physicochemical properties.

The composition of the electrode-electrolyte interface depends on the chemical mixing of the electrolyte with the cathode and the reduction stability of the electrolyte with Li metal.^[19] For example, when the LiCoO₂ cathode is paired with a garnet-type Li₇La₃Zr₂O₁₂ solid-state electrolyte, the resulting interface may include Li₂CoO₃, La₂O₃, and La₂Zr₂O₇. When a Li₂S-P₂S₅ electrolyte is used, the chemical reaction products at the LiCoO₂|Li₂S-P₂S₅ interface may include transition-metal sulfides (such as Co₉S₈, Mn₂S₃, Ni₃S₄, CoNi₂S₄) and polyanions such as PO₄³⁻ and SO₄²⁻. At the Li|solid-state electrolyte (SSE) interface, the reduction decomposition can lead to chemical reaction products such as Li_xS, Li_yP, and Li_zGe (which can form at the Li|Li_{3.25}Ge_{0.25}P_{0.75}S₄ (LGPS) interface). The electrolyte has a pivotal role in determining whether the interface between the electrode and electrolyte is suitable. In addition to the electrolyte, electrochemical reaction parameters are essential to investigate. For example, the formation cycle(s) condition the morphology and composition of the interphase between the

N.-Y. Kim, I. Kim, H.-J. Lee, Prof. J.-W. Jung
School of Materials Science and Engineering, University of Ulsan, Techno saneop-ro 55 beon-gil, Nam-gu, Ulsan 44776, Korea
E-mail: jwjung4@ulsan.ac.kr
B. Bornamehr, Prof. Dr. V. Presser
INM – Leibniz Institute for New Materials, Campus D22 66123, Saarbrücken Germany
Department of Materials Science and Engineering, Campus D22 66123, Saarbrücken Germany
E-mail: volker.presser@leibniz-inm.de
Prof. Dr. V. Presser
saarene – Saarland Center for Energy Materials and Sustainability, Campus C42 66123, Saarbrücken Germany
Dr. H. Ueda
Institute for Frontier Materials (IFM), Deakin University, 221 Burwood Highway, Burwood Victoria 3125, Australia
Battery Research and Innovation Hub, Deakin University, 5/154 Highbury Road, Burwood Victoria 3125, Australia
Dr. J. Y. Cheong
Bavarian Center for Battery Technology (BayBatt) and Department of Chemistry, University of Bayreuth, Universitätsstraße 30 95447, Bayreuth Germany
E-mail: jun.cheong@uni-bayreuth.de

 The ORCID identification number(s) for the author(s) of this article can be found under <https://doi.org/10.1002/eam2.12622>.

DOI: 10.1002/eam2.12622

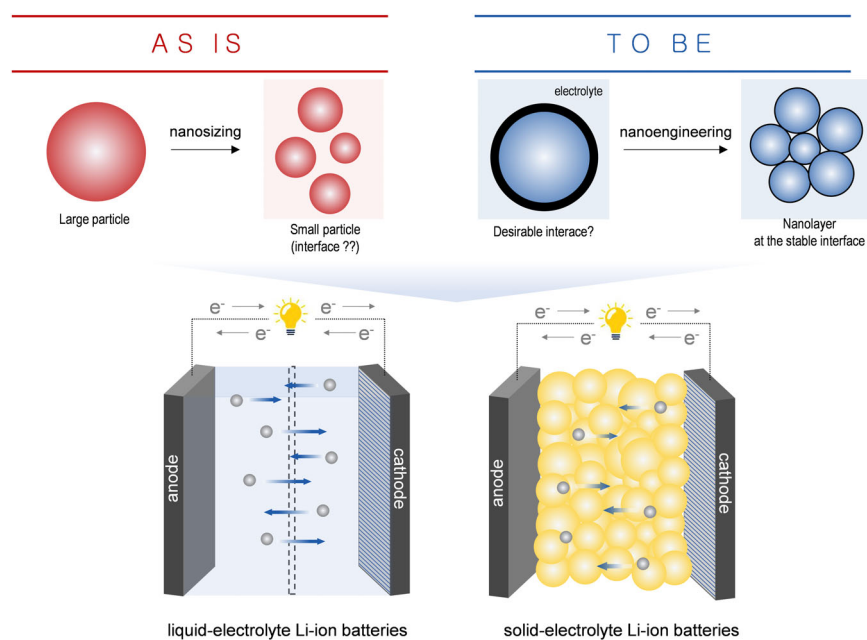


Figure 1. Schematic illustration of a desirable, nanoengineered interface between (electrode and electrode) or (electrode and electrolyte) for liquid- and solid-electrolyte Li-ion batteries.

electrolyte and electrode, where current density in the formation cycle plays a significant role in the interphase between the electrode and electrolyte, hence the electrochemical performance.^[20,21] From a recent study,^[22] electrode materials with smaller particle sizes (240 nm in the study) showed comparably good electrochemical performance compared with a particle size of 810 nm in liquid and gel-like electrolytes, where the formation of various by-products from the electrolyte degradation did not significantly affect the electrochemical performance of smaller particle sizes. This shows that the size of the electrode material particles can be a dominant factor. Nevertheless, as the interface between the electrode and electrolyte involves many factors, it is essential to control the variables to optimize the interface further. So far, most of the adopted approaches were aimed at tuning the surface characteristics of electrode material and/or electrolyte, which need to be summarized and explained further. We focused on and dealt with the interface ‘as is’ and ‘to be’ for liquid- and solid-electrolyte Li-ion batteries in this review (Figure 1).

2. Surface Modification of Interface in Electrode Materials by Nanoscale Layer

2.1. Cathode

The ever-increasing demand for rechargeable battery systems with faster charging and extended utilization requires cathode material with superior rate capabilities and cycle retention. Nanoengineered surface modification of cathode has been extensively carried out^[23] as it leads to enhanced cycle life^[24,25] and superior rate capabilities.^[26,27] In recent years, more in-depth and creative research on improving the cathode capacity has occurred by employing organic and inorganic nanoengineered surficial layers,^[24,25] which made significant research advances.

Several nanoengineered inorganic surficial layers were adopted to realize rechargeable batteries with higher energy and power density. For instance, Song et al.^[28] reported on employing a nano- AlPO_4 coating layer for $\text{Li}_{1.15}\text{Ni}_{0.17}\text{Co}_{0.11}\text{Mn}_{0.57}\text{O}_2$, enhancing the capacity. Such coating processes employ a facile in situ dispersion process, filtering, drying, and heat treatment, where heat treatment condition plays an important role in modulating the electrochemical properties of $\text{Li}_{1.15}\text{Ni}_{0.17}\text{Co}_{0.11}\text{Mn}_{0.57}\text{O}_2$. Figure 2a shows the X-ray diffractograms of the AlPO_4 -coated cathode at various heat treatment conditions, where no apparent change in the overall crystallinity was seen. Based on the elemental mapping (Figure 2b), AlPO_4 is seen on the cathode’s surface. Cycle retention (Figure 2c) and rate capabilities (Figure 2d) highlight the importance of heat treatment temperature on overall electrochemical performance: nano- AlPO_4 coating layer (at 400 °C) for $\text{Li}_{1.15}\text{Ni}_{0.17}\text{Co}_{0.11}\text{Mn}_{0.57}\text{O}_2$ (A-400) exhibits the best electrochemical performance, where the heating temperature has a significant effect on initial Coulombic efficiency, capacity decay per

cycle, and cycle retention at various C-rates. Effective coating of AlPO_4 led to surface protection of $\text{Li}_{1.15}\text{Ni}_{0.17}\text{Co}_{0.11}\text{Mn}_{0.57}\text{O}_2$, which significantly minimizes the formation of reaction by-products (LiF and LiPO_4F_2) shown by 50 cycles of charge and discharge. Similar to this concept, the hybrid surface coating was employed for $\text{LiNi}_{0.8}\text{Co}_{0.1}\text{Mn}_{0.1}\text{O}_2$ cathode using Li_3PO_4 and carbon nanotube (CNT).^[29] Here, the role of Li_3PO_4 and CNT is to improve ionic and electronic conductivity simultaneously, significantly enhancing overall electrochemical performance. Li_3PO_4 coating layer with 4 nm was deposited on NCM, and such a thin nanoscale coating layer allows facile ionic and electronic transport and ensures chemical stability against more extended exposure to air. With effective surface protection from HF corrosion, the structural integrity was well maintained for $\text{LiNi}_{0.8}\text{Co}_{0.1}\text{Mn}_{0.1}\text{O}_2$ cathode with Li_3PO_4 and CNT coating (CNT-LPO-NCM) (Figure 2e). In contrast, the pristine $\text{LiNi}_{0.8}\text{Co}_{0.1}\text{Mn}_{0.1}\text{O}_2$ cathode shows (006)/(102) and (108)/(110) split peaks that are amalgamated, indicating changes in crystalline structures (Figure 2f). Such progressive structure destruction led to a higher metal ion concentration in the electrolyte (Ni, Co, Mn) which further suggests the superior electrolyte stability for CNT-LPO-NCM. The practical role of Li_3PO_4 was also demonstrated for another cathode material (NMC811),^[30–33] where it suppresses electrolyte side reactions while alleviating crack formation after numerous cycling. For the NCM cathode (NMC811), the effects of three typical ionic conductors (Li_3PO_4 , Li_2ZrO_3 , $\text{Li}_4\text{Ti}_5\text{O}_{12}$) were further compared.^[34] The electronic and ionic conductivity improved when Li_3PO_4 was coated, leading to superior rate capabilities. Other metal oxide materials were also adopted for surface modification of the cathode, some of which include $\text{Li}_{1.4}\text{Al}_{0.4}\text{Ti}_{1.6}(\text{PO}_4)_3$,^[35,36] LiInO_2 ,^[37] Al_2O_3 ,^[38–40] Al_2O_3 and LiAlO_2 ,^[41] ZrO_2 ,^[42] LiNbO_3 ,^[43] tungsten oxide,^[44] Li_4SiO_4 ,^[45] Li_3VO_4 ,^[46] TiO_2 ,^[47] Y_2O_3 ,^[48] and SnO_2 ,^[49] and can be used for nanoscale modification in the interphase between cathode and electrolyte. Different methods for stabilizing the metal oxide coatings can be used, such as sol-gel,^[41] atomic layer

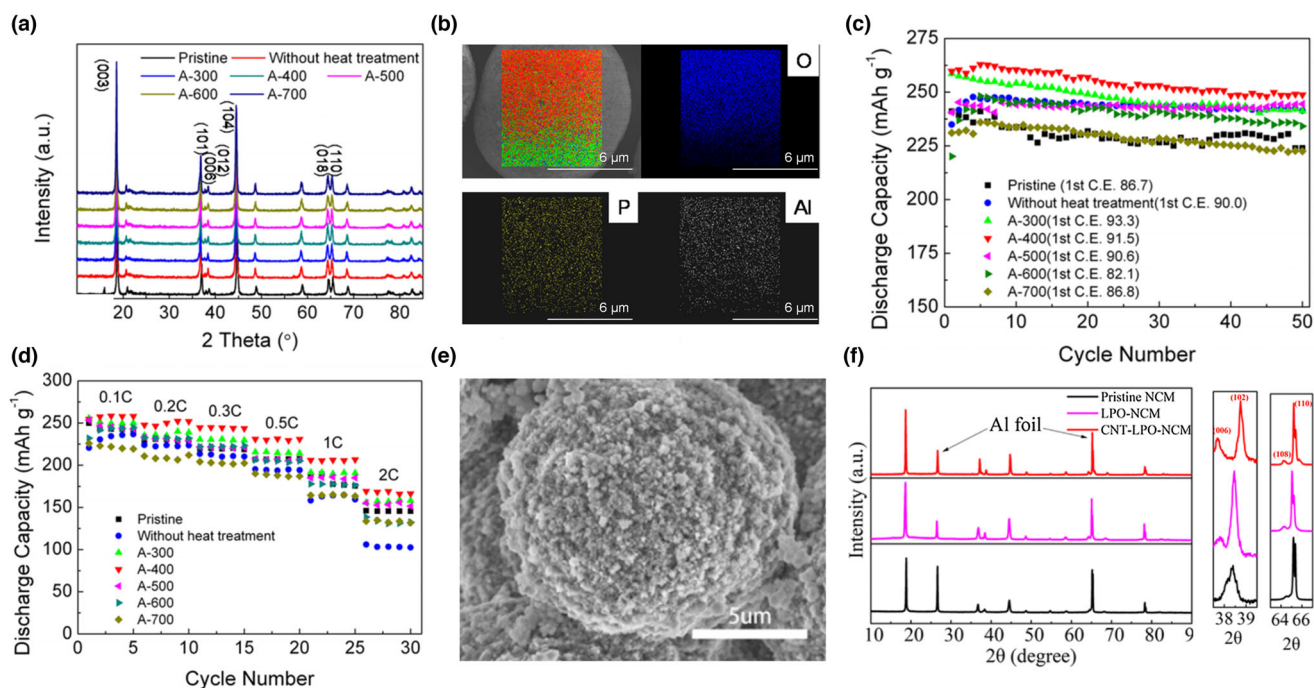


Figure 2. Microstructure and electrochemical performance of cathode with surface modification. a) X-ray diffractograms of 1% nano- AlPO_4 coated cathode at various heat treatment conditions. b) Elemental mapping of nano- AlPO_4 coated cathode at 400°C . c) Cycle retention characteristics, and d) rate capabilities of various cathode samples. Reproduced with permission.^[28] Copyright 2018, American Chemical Society. e) Scanning electron micrograph of CNT-LPO-NCM after 150 cycles. f) X-ray diffractograms of respective samples after 100 cycles. Reproduced with permission.^[29] Copyright 2019, American Chemical Society.

deposition,^[45] co-precipitation,^[48] and milling procedures such as plasma-assisted milling,^[49] and ball-milling.^[46] Usually, the aim is to deposit a Li-containing phase due to its ionic conductivity so it does not impair the rate capability. Finding the optimum coating thickness is critical for a positive effect, and thicker coatings can impede diffusion^[28] and decrease lattice matching.^[48] In most works, the improvement in the performance is correlated to the protection of the cathode material from HF attack, which is referred to as HF scavenging and restriction of direct electrode/electrolyte contact.^[38–40] This protective effect is greater at higher potentials and temperatures, at which the cathode metals are more likely to dissolve in the electrolyte.^[43] By this protection, these phases also lower the interfacial impedance,^[47] and maintain a gradual potential slope, combating the polarization at the interface^[35,36] and increasing the charge cut-off voltage.^[44]

In addition to metal oxides, metallic coatings have also shown considerable improvement in electrochemical performance regarding cycle retention and rate capabilities. For instance, highly stabilized $\text{LiNi}_{0.815}\text{Co}_{0.15}\text{Al}_{0.035}\text{O}_2$ secondary particles were achieved by introducing molybdenum (Mo),^[50] which induces a Li_2MoO_4 layer on the outer part and epitaxially grown NiO-like surface. Such coatings give rise to three critical characteristics: i) suppression of cathode-electrolyte side reactions, ii) prevention of structural degradation, and iii) minimization of intergranular cracking. Just with 1 mol % of surficial Mo coating, it shows outstanding rate capabilities (140 mAh g^{-1} at 10C) and cycle retention characteristics (95.7% at 5C after 250 cycles). In addition to Mo, other metals/metal halides and metal sulfides were also doped on the surface of cathodes, such as Zr,^[51,52] MoS_2 ,^[53] LiAlF_4 ,^[54] and S.^[55] Moreover, co-doping of metals and/or metal sulfides/halides were also

adopted to improve the electrochemical performance, such as Na and F,^[56] Cd and S,^[57] and F and LiF.^[58] Instead of using similar elements/compounds, metal and metal oxide surficial modifications were employed simultaneously for some cathodes, including Ti and $\text{La}_4\text{Ni-LiO}_8$.^[59] With a significant change in structural features, a double-shell hybrid nanostructure was also employed for electrochemical performance, the example of which is combining a Li_2SiO_3 coating layer and a cation-mixed layer ($\text{Fm}\bar{3}\text{m}$ phase) and coating them on the surface of NCM811.^[60] With the introduction of a Li_2SiO_3 coating layer (<10 nm), cation-mixed layer increased from 1–2 nm to 5–6 nm, which led to the interfacial stability and structural integrity. Carbon@spinel@layered@spinel@carbon shells that were employed for Li-rich layered oxides,^[61] retaining discharge capacities of 228 and 196 mAh g^{-1} at 1C and 5C, respectively, after 200 cycles. These multi-layer coatings aim to improve the electrochemical performance by increasing the ionic transport, and improving the structural stability.

In addition to the above-mentioned inorganic species, polymer coatings have also been employed to overcome the shortcomings of the inorganic coating layer. For example, constructing a poly(acrylonitrile-co-butadiene) surface layer on a $\text{LiNi}_{0.6}\text{Mn}_{0.2}\text{Co}_{0.2}\text{O}_2$ cathode significantly improved electrochemical performance.^[62] Here, the polymeric surficial layer suppresses side reactions by enlarging the physical contact at solid electrode/solid electrolyte interfaces from points to larger areas during the cycling process and decreasing the interfacial resistance. This resulted in higher cycle retention (75% cycle retention over 400 cycles) and rate capabilities (99 mAh g^{-1} at a rate of 3C) compared to the unprotected cathode. Similarly, a protective conductive polymer (poly(3,4-ethylene dioxithiophene)) was used to coat Ni-rich cathodes

highly conformally.^[63] As a result, it facilitates the transfer of ions and electrons, suppresses the undesired layered to spinel/rock-salt phase transformation, and mitigates intergranular/intragranular mechanical cracking.^[63] In addition, other conductive polymers, such as polyaniline (PANI), have been used as a coating to create a physical barrier between the cathode and the electrolyte.^[64] A 5–7 nm thin PANI layer was uniformly coated onto the Ni-rich NCM811, which effectively hindered side reaction and improved the interface between electrode and electrolyte. PANI has also been co-polymerized with ionically conductive poly(ethylene glycol) to create a homogeneous coating.^[65] A homogeneous and amorphous layer with a thickness of 25–30 nm and 30–35 nm was observed with PANI and PANI/poly(ethylene glycol) composite film, which was sufficient to ensure high ionic conductivity and maintain structural integrity. In contrast to the inorganic coating, these organic counterparts can mitigate the volumetric expansion during cycling, avoid pulverization, and increase the mechanical stability of the cathode material due to their flexibility.^[65] On top of these research advances, Yoon et al.^[66] recently reported a nano-scale Co_xB protective layer on the surface and grain boundary of NCM, which greatly improved the electrochemical performance. This work is important in that interface was controlled at the grain boundary level, where uniform interfaces in both grain boundary and boundaries between primary particles cathode are also necessary to ensure enhanced electrochemical performance.

In summary, inorganic and organic nanoscale coating layers were used for the cathode, and some hybrid inorganic/organic surficial coating layers have been explored. The thickness of the nanoengineered layer was usually below 10 nm, a thin layer that prevented side reactions and contributed to enhanced interfacial stability while allowing facile ionic transport since ionic conductivity is indispensable for the electrochemical performance of the cathode. Many of these studies hint at the importance of nanoscale interfacial engineering on the cathode part, significantly improving the electrochemical performance and properties.

2.2. Anode

From a practical perspective, surface modifications must be applied to micrometer-sized anode particles in contrast to the nanosized anode particles, as the former exhibits higher tap density. For example, Wang et al.^[67] deposited a thin Si coating followed by a graphene cage on Si microparticles (Mp-Si@Si@G), which greatly enhanced the interface between anode and electrolyte and enhanced the electrochemical performance. The Si coating was about 100 nm thick, while the outermost graphene cage coating was only ~7 nm, which were employed as double layers to alleviate the volume changes of Si effectively. The schematic illustration of the fabrication of Mp-Si@Si@G is presented in **Figure 3a**, which undergoes annealing, etching, Si coating, and graphene coating.

To compare the dynamic changes on the interface of the anode, Si microparticles (pristine sample) and Mp-Si@Si@G were analyzed for in situ transmission electron microscopy analysis (Figure 3b–e). Crack formation is observed in the Si microparticles, which leads to an unstable interface between them and the electrolyte. The interface and structure of Mp-Si@Si@G are well maintained during and after lithiation. It is further verified that Si skin lowers the unfavorable electrolyte/electrode contact area and minimizes SEI layer formation for Mp-Si@Si@G, resulting in much superior cycle retention (Figure 3f).

Although Si is actively researched due to its high theoretical capacity (ten times higher than the theoretical capacity of graphite), other anode materials such as graphite are also researched. Tallman et al.^[68] sputtered Cu and Ni nanoscale layers on the graphite to increase the overpotential for Li deposition, thereby suppressing Li plating under high-rate charge conditions. Deposition overpotential can be increased by modifying the graphite interface, which significantly reduces the quantity of plated Li metal by 50%. Heng et al.^[69] suggested a functional film (nano 2,2-dimethylethenylboronic acid) on natural graphite, which greatly enhanced the cycling stability of graphite when it is assembled in a full cell (with $\text{LiNi}_{0.5}\text{Co}_{0.2}\text{Mn}_{0.3}\text{O}_2$ as a cathode). Although the thickness of the film was only about 20 nm, it built a stable

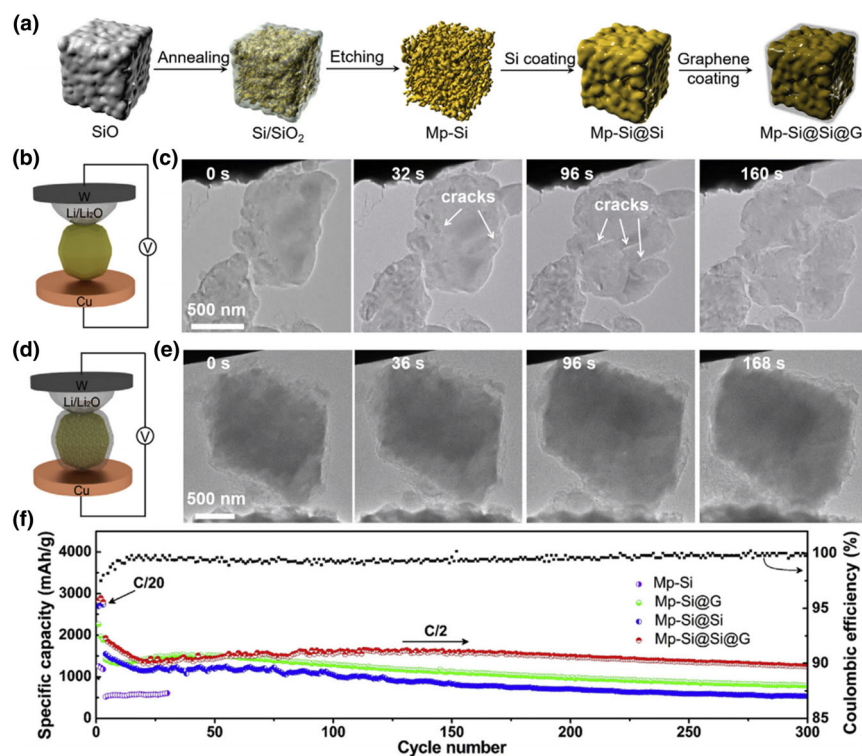


Figure 3. Microstructure and electrochemical performance of anode with surface modification. a) Schematic illustration of the synthesis of graphene cage-encapsulated Si skin-sealed mesoporous Si microparticles (Mp-Si@Si@G). b) Schematic illustration of the in-situ TEM setup for the Si microparticles. c) Time-series TEM snapshots of Si microparticles. d) Schematic illustration of in situ TEM setup of Mp-Si@Si@G. e) Time-series TEM snapshots of Mp-Si@Si@G. f) Capacity retention characteristics of mesoporous Si microparticles (Mp-Si), graphene cage-Si microparticles (Mp-Si@G), Si sealed mesoporous Si (Mp-Si@Si), and Mp-Si@Si@G. Reproduced with permission.^[67] Copyright 2019, Elsevier.

Table 1. Summary of nanoscale layer on electrode materials by surface modification.

Electrode material	Coating material	Method	Layer thickness	References
$\text{Li}_{1.15}\text{Ni}_{0.17}\text{Co}_{0.11}\text{Mn}_{0.57}\text{O}_2$	AlPO_4	Co-precipitation	5–15 nm	[28]
$\text{LiNi}_{0.8}\text{Co}_{0.1}\text{Mn}_{0.1}\text{O}_2$	Li_3PO_4 , carbon nanotube (CNT)	Co-precipitation	4 nm	[29]
$\text{LiNi}_{0.8}\text{Co}_{0.1}\text{Mn}_{0.1}\text{O}_2$	Li_3PO_4	Hydrothermal synthesis	2–4 nm	[34]
$\text{LiNi}_{0.8}\text{Co}_{0.1}\text{Mn}_{0.1}\text{O}_2$	Li_2ZrO_3	Hydrothermal synthesis	2–4 nm	[34]
$\text{LiNi}_{0.8}\text{Co}_{0.1}\text{Mn}_{0.1}\text{O}_2$	$\text{Li}_4\text{Ti}_5\text{O}_{12}$	Hydrothermal synthesis	2–4 nm	[34]
$\text{LiNi}_{0.6}\text{Co}_{0.2}\text{Mn}_{0.2}\text{O}_2$	$\text{Li}_{1.4}\text{Al}_{0.4}\text{Ti}_{1.6}(\text{PO}_4)_3$	Sol-gel method	6 nm	[35]
LiCoO_2	$\text{Li}_{1.4}\text{Al}_{0.4}\text{Ti}_{1.6}(\text{PO}_4)_3$	Solid-state synthesis	~20 nm	[36]
$\text{LiNi}_{0.8}\text{Co}_{0.1}\text{Mn}_{0.1}\text{O}_2$	$\text{In}_2\text{O}_3\&\text{LiInO}_2$	Co-precipitation	12 nm	[37]
$\text{Li}_{1.256}\text{Ni}_{0.198}\text{Co}_{0.082}\text{Mn}_{0.689}\text{O}_{2.25}$	Al_2O_3	Co-precipitation	3 nm	[38]
$\text{LiNi}_{0.6}\text{Co}_{0.2}\text{Mn}_{0.2}\text{O}_2$	Al_2O_3	Atomic layer deposition	1–4 nm	[39]
$\text{LiNi}_{0.6}\text{Co}_{0.2}\text{Mn}_{0.2}\text{O}_2$, $\text{LiNi}_{0.8}\text{Co}_{0.15}\text{Al}_{0.05}\text{O}_2$	Al_2O_3	Atomic layer deposition	5–10 nm	[40]
$\text{LiNi}_{0.6}\text{Co}_{0.2}\text{Mn}_{0.2}\text{O}_2$	LiAlO_2	Sol-gel method	1 nm	[41]
$\text{LiNi}_{0.6}\text{Co}_{0.2}\text{Mn}_{0.2}\text{O}_2$	ZrO_2	Solvothermal synthesis/ball-milling	5 nm	[42]
$\text{LiNi}_{0.8}\text{Co}_{0.1}\text{Mn}_{0.1}\text{O}_2$	LiNbO_3	Co-precipitation	5–6 nm	[43]
$\text{LiNi}_{0.8}\text{Co}_{0.1}\text{Mn}_{0.1}\text{O}_2$	$\text{Li}_2\text{WO}_4/\text{WO}_3$	Sol-gel method	—	[44]
$\text{LiNi}_{0.8}\text{Co}_{0.15}\text{Al}_{0.05}\text{O}_2$	Li_4SiO_4	Co-precipitation/solid-state method	2–5 nm	[45]
$\text{LiNi}_{0.6}\text{Co}_{0.2}\text{Mn}_{0.2}\text{O}_2$	Li_3VO_4	Ball-milling	6–10 nm	[46]
$\text{LiNi}_{0.6}\text{Mn}_{0.2}\text{Co}_{0.2}\text{O}_2$	TiO_2	Atomic layer deposition	—	[47]
$\text{Li}_{1.2}\text{Mn}_{0.54}\text{Ni}_{0.13}\text{Co}_{0.13}\text{O}_2$	Y_2O_3	Co-precipitation	5–10 nm	[48]
$\text{LiNi}_{0.5}\text{Co}_{0.2}\text{Mn}_{0.3}\text{O}_2$	SnO_2	Plasma-assisted ball-milling	—	[49]
$\text{LiNi}_{0.5}\text{Co}_{0.2}\text{Mn}_{0.3}\text{O}_2$	Li_2MoO_4	Co-precipitation	—	[50]
$\text{LiNi}_{0.8}\text{Co}_{0.1}\text{Mn}_{0.1}\text{O}_2$	Li_2ZrO_3	Co-precipitation	—	[51]
LiNiO_2	Li_2ZrO_3	Co-precipitation	5–10 nm	[52]
$\text{LiNi}_{0.8}\text{Co}_{0.1}\text{Mn}_{0.1}\text{O}_2$	MoS_2	Co-precipitation	14–16 nm	[53]
$\text{Li}_{1.2}\text{Ni}_{0.2}\text{Mn}_{0.6}\text{O}_2$	LiAlF_4	Co-precipitation	5 nm	[54]
$\text{LiNi}_{0.5}\text{Mn}_{1.5}\text{O}_4$	S	Co-precipitation	—	[55]
$\text{LiNi}_{0.6}\text{Co}_{0.2}\text{Mn}_{0.2}\text{O}_2$	Na, F	Co-precipitation	—	[56]
$\text{Li}_{1.2}\text{Ni}_{0.2}\text{Mn}_{0.6}\text{O}_2$	Cd, S	Co-precipitation	—	[57]
$\text{LiNi}_{0.5}\text{Co}_{0.2}\text{Mn}_{0.3}\text{O}_2$	F, LiF	Co-precipitation	—	[58]
$\text{LiNi}_{0.8}\text{Co}_{0.1}\text{Mn}_{0.1}\text{O}_2$	Ti, $\text{La}_4\text{NiLiO}_8$	Co-precipitation	—	[59]
$\text{LiNi}_{0.8}\text{Co}_{0.1}\text{Mn}_{0.1}\text{O}_2$	Li_2SiO_3	Co-precipitation	—	[60]
$\text{LiNi}_{0.8}\text{Co}_{0.1}\text{Mn}_{0.1}\text{O}_2$	Carbon, LiMn_2O_4	Co-precipitation	100 nm	[61]
$\text{LiNi}_{0.6}\text{Mn}_{0.2}\text{Co}_{0.2}\text{O}_2$	Poly(acrylonitrile-co-butadiene) (PAB)	UV polymerization	~10 nm	[62]
$\text{LiNi}_{0.33}\text{Co}_{0.33}\text{Mn}_{0.33}\text{O}_2$, $\text{LiNi}_{0.85}\text{Co}_{0.1}\text{Mn}_{0.05}\text{O}_2$, $\text{Li}_{1.2}\text{Mn}_{0.54}\text{Ni}_{0.13}\text{Co}_{0.13}\text{O}_2$	Poly(3,4-ethylenedioxythiophene) (PEDOT)	Chemical vapor deposition	7–28 nm	[63]
$\text{LiNi}_{0.8}\text{Co}_{0.1}\text{Mn}_{0.1}\text{O}_2$	Poly(vinylpyrrolidone) (PVP), Polyaniline (PANI)	Co-precipitation	5–7 nm	[64]
$\text{LiNi}_{0.8}\text{Co}_{0.1}\text{Mn}_{0.1}\text{O}_2$	Polyaniline (PANI), Polyethylene glycol (PEG)	Co-precipitation	25–35 nm	[65]
$\text{LiNi}_{0.8}\text{Co}_{0.1}\text{Mn}_{0.1}\text{O}_2$	Co_xB	Co-precipitation	~5 nm	[66]
Si	Si, Graphene	Ball-milling, Chemical vapor deposition	107 nm	[67]

SEI layer on the graphite through the in-situ self-polymerization of nano 2,2-dimethylethenylboronic acid molecules. These works demonstrate that the nanoscale surface protection layer helps to build a more stable interface between electrode and electrolyte.

Surface modification was also adopted for Li metal, which exhibits high theoretical capacity (3860 mAh g^{-1}), low density (0.534 g cm^{-3}), and low electrical potential (-3.04 V vs. standard hydrogen electrode).^[66] Li dendrite growth, rupture of the SEI layer, and formation of dead Li contribute to the rapid decay in the electrochemical performance of Li metal,^[70] and some approaches were aimed at tuning the surface properties of Li metal. For instance, a 20-nm-thin Al_2O_3 layer was coated onto the Li metal by sputter coating, which is a simple coating method.^[71] The ionic conductivity of LiAlO_2 was measured as $10^{-7} \text{ S cm}^{-1}$, providing both surface chemical stability and suppression of dendritic growth. Chen et al.^[72] employed LiF coating on Li metal by atomic layer deposition, where a thickness of 8 nm was achieved. Crystalline LiF films achieved a shear modulus of 58 GPa, which is seven times higher than the sufficient value to prevent Li dendritic growth. LiF coating led to a stable Coulombic efficiency of 99.5% over 170 years. In addition to single-layer surface protection, a dual-layer film (organic components such as ROCO_2Li and ROLi on top

(estimated to be 25 nm) and inorganic components such as Li_2CO_3 and LiF on the bottom (estimated to be 50 nm)) was coated onto the Li metal to protect it from the corrosion and regulate the uniform deposition of Li.^[73] It led to a dendrite-free deposition of Li metal, longer cycling stability in symmetric and asymmetric cells, and smaller interfacial polarization (360 mV for dual-layer-film-coated Li metal and 590 mV for reference at a current density of 5.0 mA cm^{-2}). In contrast to surface modification (nanoscale surficial layer) on the cathode, the thickness of the surficial layer on the anode tends to be much larger (sometimes sub-micrometer scale: 100 nm; **Table 1**). Such thicker nanolayers can be attributed to the fact that anode materials (such as Si) tend to undergo massive volume changes ($>300\%$) and morphological evolution (such as the formation of Li dendrites), where thicker nanoscale interphase between electrode and electrolyte is desired.

2.3. Solid Electrolyte

Several recent studies provide an optimized interface between electrodes and the electrolyte through solid electrolyte modification. Among various types of solid electrolytes, $\text{Li}_7\text{La}_3\text{Zr}_2\text{O}_{12}$ (LLZO) is one of the most

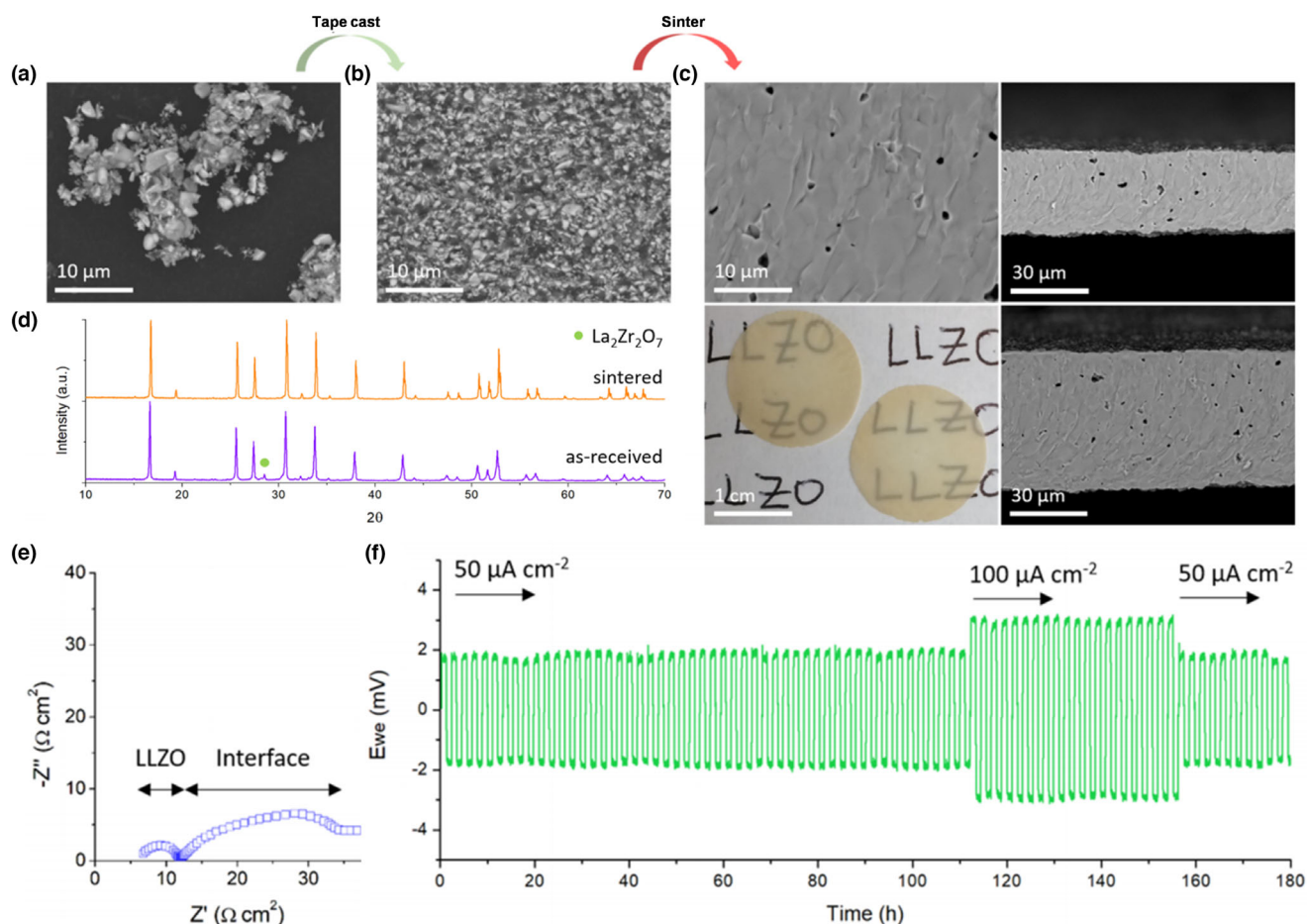


Figure 4. Microstructure and electrochemical performance of LLZO. Scanning electron micrographs of a) LLZO powder and b) fracture surface of tape-cast green tape. c) SEM and optical images of LLZO films sintered in optimal sintering profile. d) X-ray diffractograms of sintered and as-received LLZO film. e) Impedance test (Nyquist plot) and f) DC cycling of Au interface engineered Li/LLZO/Li cell. Reproduced with permission.^[74] Copyright 2020, American Chemistry Society.

promising metal oxide-based solid electrolytes, and much work has been devoted to improving its surficial properties. Recently, Al-substituted LLZO combined with the cathode featuring dual layers (dense LLZO membranes and porous LLZO scaffolds) infiltrated with $\text{LiNi}_{0.6}\text{Mn}_{0.2}\text{Co}_{0.2}\text{O}_2$ while using Li as the counter electrode has been reported.^[74] In this work, tape casting followed by sintering resulted in dense LLZO membranes (Figure 4a–c). X-ray diffraction (Figure 4d) shows that the crystalline peak related to $\text{La}_2\text{Zr}_2\text{O}_7$ disappeared, indicating more crystalline peaks after the sintering process. Electrochemical properties of LLZO were characterized by electrochemical impedance spectroscopy (Nyquist plot, Figure 4e) and electrochemical cycling (Figure 4f) using a Li/LLZO/Li cell configuration. Based on the impedance test, LLZO exhibits an overall cell impedance of $35 \Omega \text{ cm}^2$, while an interfacial impedance is only $12 \Omega \text{ cm}^2$, much lower than previously reported values.^[75,76] As a result, LLZO can stably be cycled at current densities of 50 and $100 \mu\text{A cm}^{-2}$, which leads to stable electrochemical reactions having discharge capacities of 125–135 mAh g^{-1} .

Hybrid polymer-inorganic electrolytes can also induce a suitable interface between the electrode and electrolyte, especially at the cathode–solid–electrolyte interface. Wu et al.^[77] reported functional composite polymer electrolytes with imidazole-modified SiO_2 nanoparticles (300 nm), where a combinatorial effect of both SiO_2 and polyvinylidene fluoride (PVDF)/polyethylene (PE) is present. When imidazole-modified SiO_2 nanoparticles are used, they lead to a more compact and uniform cathode electrolyte interphase (7.5 nm), reducing interfacial resistance and improving cycle retention.^[77] SiO_2 acted as a water/acid scavenger and filler for electrolytes, leading to an increase in charge cut-off voltage to 4.5 V. Another enhanced method is the so-called tri-layer strategy to improve the contact between the electrode and the electrolyte effectively. For example, Zhang et al.^[78] employed a three-dimensional $\text{Li}_{1.5}\text{Al}_{0.5}\text{Ge}_{1.5}(\text{PO}_4)_3$ (LAGP) layer made by templating to form a porous structure that hosts the cathode material by infiltration. This electrolyte is an ionically conductive thin and dense layer that can block dendrite growth. After the cathode addition, the last component is polyethylene glycol bis(amine)-triglycidyl isocyanurate. This solid-state cross-linked polymer fills the gaps between the former two to increase their contact. This compact design maximized cathode loading up to 13 mg cm^{-2} , delivering an areal capacity of 2 mAh cm^{-2} at a rate of 0.1C with a capacity retention of 70% after 50 cycles. Composite solid electrolytes were also recently developed with much progress, some of which include $\text{Li}_3\text{BO}_3\text{-Li}_{6.4}\text{La}_3\text{Zr}_{1.4}\text{Ta}_{0.6}\text{O}_{12}$,^[79] $\text{PEO}_{20}\text{-LiTFSI-Li}_6\text{PS}_5\text{Cl}$,^[80] $\text{Li}_6\text{PS}_5\text{Cl/poly(ethylene oxide)}$,^[81] tantalum-doped lithium lanthanum zirconium oxide,^[82] and poly(ethylene oxide)- $\text{LiClO}_4\text{-Li}_{1.3}\text{Al}_{0.3}\text{Ti}_{1.7}(\text{PO}_4)_3$.^[83] Although the solid electrolyte itself is not nanoscale, adopting proper solid electrolyte results in an enhanced interface between electrode and electrolyte. It can be in nanoscale interphase that contributes to more interfacial stability.

3. Tuning the Interface by Formation of a Solid Electrolyte Interphase Layer

3.1. By Introducing an Artificial Interphase

Forming an artificial solid interphase is a powerful concept for tuning the interface and improving the electrochemical performance. This creates an electrolyte interphase layer on the electrode before cell assembly, which artificially mitigates and solves several issues raised in the conventional LIBs configurations. For instance, an artificial interphase layer

on a cathode material, such as Ni-rich NCM,^[84] can comprise silyl ether functional groups. The latter can be formed by employing wet-coating-based thermal treatment, using dimethoxy-dimethyl silane as an organic solvent. Through in-depth analysis, it has been found that Si-O functional groups were effective in F^- scavenging, leading to fewer side reactions. The as-formed electrode–electrolyte interphase layer improved the interfacial stability of the Ni-rich NCM cathode, leading to higher cycle retention. Jang et al.^[85] formed a chemically induced interphase layer by employing lithium tetra(trimethylsilyl) borate as a functional precursor. The formed coating layer was about 5–8 nm, improving interfacial stability and scavenging fluoride species. Silyl-borate functional groups in the precursor greatly minimize the electrolyte decomposition (along with side reactions) and scavenge fluoride species. Simulation data suggest that it is thermodynamically favorable for lithium tetra(trimethylsilyl) borate to bond to fluoride species, thus mitigating the electrolyte decomposition. As a result, the cell employing such an artificial interphase layer shows stable cycling at a high temperature of 55°C after 100 cycles.

The formation of an artificial interphase layer has also been adopted for anodes, particularly in the case of Li metal. For instance, Li et al.^[86] employed garnet-type $\text{Li}_{6.4}\text{La}_3\text{Zr}_{1.4}\text{Ta}_{0.6}\text{O}_{12}$ (LLZTO)-based artificial interphase layer onto the Cu current collector, where the interphase layer greatly reduces the contact between Li and electrolyte. When sintering the LLZTO together with the Cu current collector, interdiffusion of Cu and Ta_2O_5 takes place, fixing an LLZTO layer on the Cu current collector. Such formation of an artificial interphase layer leads to enhanced Li plating/stripping performance, a long lifespan of 2400 h = 100 days, high rate capabilities with a maximum current density of 20 mA cm^{-2} , and a high areal capacity of 8 mAh cm^{-2} for 100 cycles. Various materials were selected as an artificial interphase layer for Li metal, some of which include covalent organic framework,^[87] $[\text{LiNBH}]_n$ chains,^[88] PIM-1,^[89] LiBAMB-PETMP,^[90] metal–organic framework,^[91] graphene oxide,^[92] carbon nitride/graphene/carbon nitride,^[93] and antimony-doped lithium phosphate.^[94] Furthermore, an artificial interphase layer has also been adopted in other prospective anode materials, such as Si.^[95–98]

Many of these established artificial interphases are thinner than 10 nm and uniform (Table 2), which can effectively prevent the side reaction and enhance interfacial stability. However, also micrometer-sized artificial interphase layers were adopted onto the anode (Cu, Li).^[86,89–92] This showed that both micrometer-scale and nanoscale artificial interphase layers have been adopted onto the anode to improve surface properties, ion and electron transport, and structural integrity after galvanostatic cycling.

3.2. By Introducing Additives

Modulating the electrode/electrolyte interphase is very important to obtain high energy density LIBs,^[99] and such an approach can only be employed by preparing the rationally designed electrolyte, forming a tailored solid electrolyte interphase (SEI) layer. In a typical lowest unoccupied molecular orbital (LUMO) – highest occupied molecular orbital (HOMO) diagram of the electrolyte,^[100] an anode works as a reductant while a cathode works as an oxidant. The gap between the LUMO and HOMO levels is translated to the operation window of the electrolyte and the cell potential window can be calculated. The SEI layer is built at the electrochemical potential of the anode at energies above the LUMO level. Similarly, cathode–electrolyte interphase (CEI) forms at the

Table 2. Summary of interphase layer on electrode materials by artificial interphase layer.

Electrode material	Coating material	Method	Layer thickness	References
DODSi-LiNi _{0.8} Co _{0.1} Mn _{0.1} O ₂	Di-methoxydimethylsilane (DODSi)	Wet-Coating	1%coating – 5.0 nm 2% coating-6.5 nm 10% coating-7.5 nm	[84]
0.05 LTB-LiNi _{0.8} Co _{0.1} Mn _{0.1} O ₂	Lithium tetra(trimethylsilyl) borate(LTB)	Rotary evaporation	5–8 nm	[85]
Cu foil-LLZTO	Li _{6.4} La ₃ Zr _{1.4} Ta _{0.6} O ₁₂ (LLZTO)	Dispersed on and heat treatment	10–20 μm	[86]
COF _{TAPB-PDA} -Li	1,3,5-tris(4-aminophenyl)benzene (TAPB)-terephthaldehyde (PDA)	Filtration	10 nm	[87]
Li@[LiNBH]n	[LiNBH]n layer	Immersed/Heated/cooled/washed and evaporation	140–160 nm	[88]
Li@PIM-1	PIM-1 (polymer of intrinsic microporosity)	Stirred/vacuumed/ dried	4.4 μm	[89]
LP-Li	LiBAMB-PETMP (LP)	Drop casting/ultraviolet expose/dry	1.8 μm	[90]
Cu@Zn-MOF/PVA	Zn-metal organic framework (MOF)/polyvinyl alcohol (PVA)	Spin coating	3.1 μm	[91]
Cu@GO	Graphene oxide (GO)	Spin coating	1.2 μm	[92]
g-C ₃ N ₄ /G/Cu	g-C ₃ N ₄ /graphene/g-C ₃ N ₄	Self-assembly and in-situ calcination reaction	8 nm	[93]
Cu-Sb-doping Li ₃ PO ₄	Sb-doped Li ₃ PO ₄	Radio frequency magnetron sputtering	100 nm	[94]
Si@COF	Covalent organic framework (COF)	Frozen/heating/filtration	5 nm	[95]
Si@LiAlO ₂	LiAlO ₂	Stirring/centrifugation/dry	2 nm	[96]
Si/SiO _x -PBS	Poly(borosiloxane) (PBS)	Drop-casted	—	[97]
P-SiOx@PTN	Poly-tannins (PTN)	Etching and drying	50–100 nm	[98]

potential of the cathode below the HOMO energy level, thus widening the stable potential window.^[100] For example, Cheng et al.^[101] recently suggested a novel inorganic/polymer CEI by in situ electrochemical oxidation of trace amounts of dual additives. By employing lithium bis(oxalate)borate (LiBOB) and dopamine (DA) as the dual additives, both the cycle retention characteristics and rate capabilities were significantly improved (Figure 5a,b), which could be ascribed to the formation of different interfacial layers. Schematic illustrations of the cathode without and with LiBOB + DA (Figure 5c,d) suggest that a uniform CEI is formed in the case of LiBOB + DA with only a layered phase, different

from conventional electrolyte showing non-uniform CEI with layered and rock-salt phases. The outer layer of the cycled particles in the conventional electrolyte is 20 nm thick. In comparison, that of cycled particles in the modified electrolyte is 2 nm thick, which leads to more facile ionic transport. Furthermore, it protects the cathode from harmful side reactions and phase transition to rock-salt phases, leading to facile Li⁺ ion diffusion.^[101]

Based on experimental evidence and theoretical estimations, a more optimized combination of electrolyte additives can be investigated. Kim et al.^[102] employed 3-(trimethylsilyl)-2-oxazolidinone (TMS-ON), which prevents the hydrolysis of LiPF₆ and scavenges HF in the electrolyte. Both experimental and theoretical analyses were combined to demonstrate the superiority of using TMS-ON. The general issues related to the hydrolysis of LiPF₆ and the formation of reactive species are illustrated in Figure 6a, despite the controversy of whether the water content has detrimental effects on cell performance.^[103,104] LiPF₆, one of the most frequently used salts in the electrolyte, can undergo autocatalytic decomposition to form LiF and PF₅. The formed PF₅ can severely damage the SEI layer formed on the surface of the electrode. Additionally, PF₆⁻ produced by dissociation of LiPF₆ in the electrolyte can react with water to produce HF, which further leaches the transition metal from the cathode and strongly affects the SEI layer.^[102] Therefore, TMS-ON was employed to improve the quality of the SEI layer further. PF₅ stabilizing effects

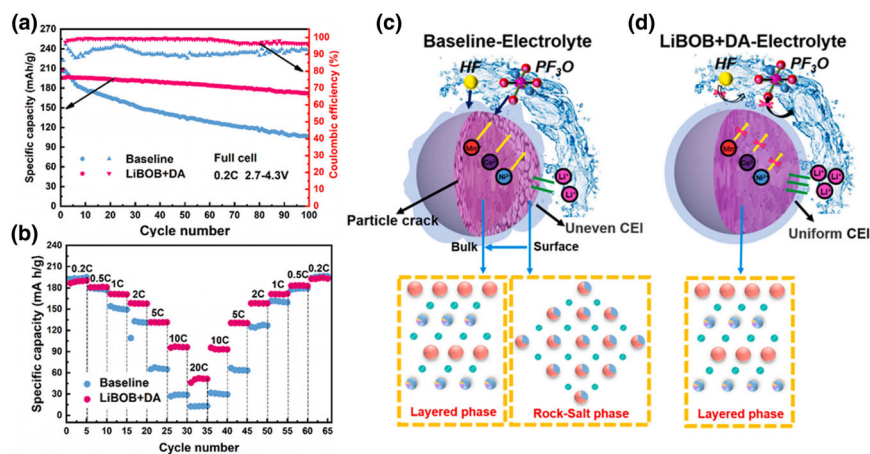


Figure 5. Electrochemical performance and schematic illustration of CEI layer. a) Cycle performance and b) rate capabilities of electrolyte with and without LiBOB + DA. Schematic illustration of the formation of the CEI layer and different phases c) without and d) with LiBOB + DA. Reproduced with permission.^[101] Copyright 2021, Elsevier.

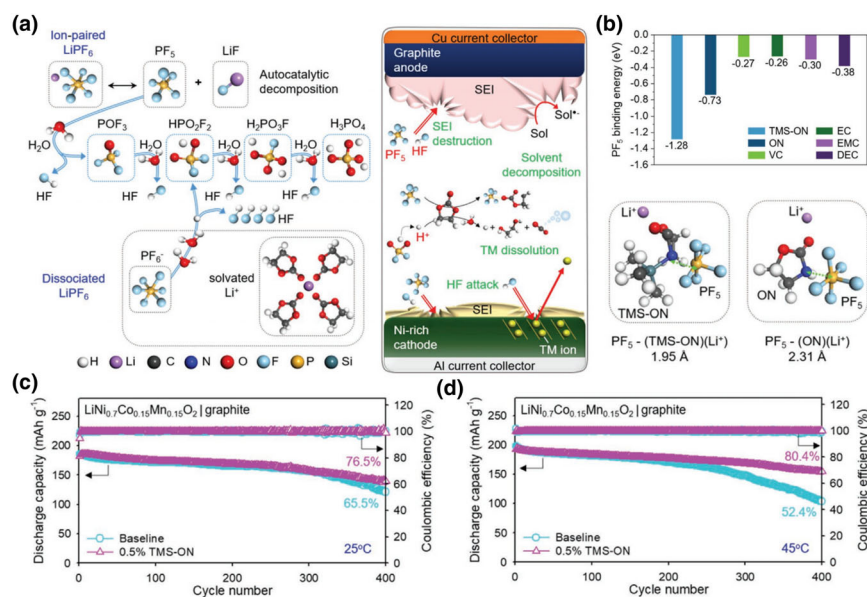


Figure 6. Theoretical and experimental investigation on electrolyte additives. a) Schematic illustration of the chemical decomposition of LiPF₆ (acidic components + reactive species) and related problems. b) PF₅ binding energies of various components coordinated with Li⁺. Cycle retention characteristics of LiNi_{0.7}Co_{0.15}Mn_{0.15}O₂/graphite full cells in a baseline electrolyte and 0.5% (trimethylsilyl)-2-oxazolidinone electrolyte at c) 25 °C and d) 45 °C. Reproduced with permission.^[97] Copyright 2020, Wiley.

by various solvents were theoretically investigated by density functional theory (DFT) calculations (Figure 6b).^[102] TMS-ON shows the highest PF₅ binding energies among 2-oxazolidinone (ON), vinylene carbonate (VC), ethylene carbonate (EC), ethyl methyl carbonate (EMC), and diethyl carbonate (DEC), which suggests that PF₅ binds more strongly

current research is aimed toward solid-state lithium batteries replacing lithium-ion batteries, the research interests in tuning the interface and interphase between electrode and electrolyte are becoming more critical (Scheme 1). Based on the literature,^[110–114] the following points can be concluded and suggested:

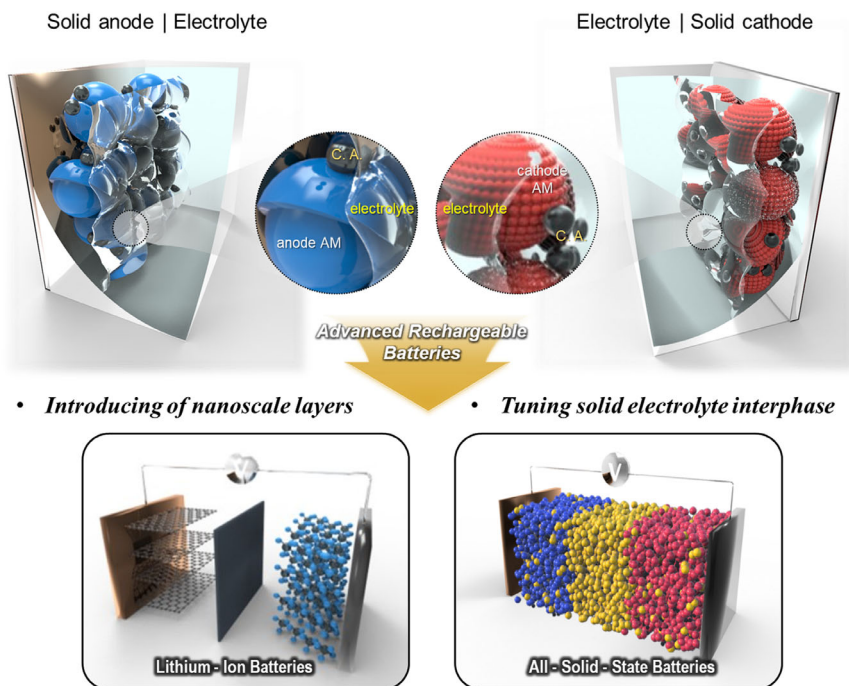
to TMS-ON rather than to the conventional electrolyte. The binding distance of TMS-ON is also very short (1.95 Å), due to the electron-donating nature of TMS functional groups.^[102] Attributed to these characteristics, electrolyte with TMS-ON leads to superior cycle retention both at room temperature (Figure 6c) and 45 °C (Figure 6d). Some other materials were also employed as additives for electrolytes, including Al₂O₃ nanofibers,^[105] Lithium difluorophosphate (LiDFP),^[106] bis(trimethylsilyl)carbodiimide,^[107] N-Allyl-N,N-bis(trimethylsilyl)amine,^[108] and 1-(2-cyanoethyl) pyrrole.^[109] A number of these additives in the electrolytes contribute to the formation of an ultrathin, nanoscale interfacial layer on the electrode (Table 3), which leads to facile ionic and electron transport.

4. Conclusions and Outlook

The interface and interphase between the electrode and electrolyte are essential aspects of research and investigation for various types of batteries, as they are critical to ensure facile ion and electron transport and to improve the state of health in the battery. Especially as the

Table 3. Summary of interphase layer on electrode materials by electrolyte additives.

Electrode material (cathode/anode)	Electrolyte	Additive	CEI/SEI layer thickness (cycles)	References
LiNi _{0.8} Co _{0.1} Mn _{0.1} O ₂ / Graphite	1.4 M Lithium bis(fluorosulfonyl)imide (LiFSI) in dimethyl carbonate (DMC)-ethylene carbonate (EC)-1,1,2,2-tetrafluoroethyl-2,2,3,3-tetrafluoropropyl ether (TTE) (2:0.2:3 by mol)	1,1,2,2-tetrafluoroethyl-2,2,3,3-tetrafluoropropyl ether (TTE)	3 nm/1 nm (100)	[99]
LiNi _{0.8} Co _{0.1} Mn _{0.1} O ₂ /Li	1.1 M Lithium hexafluorophosphate (LiPF ₆) in ethylene carbonate (EC) – diethylene carbonate (DEC) (1:1 by volume)	0.1 M lithium bis oxalate (LiBOB) + 0.1 mass% dopamine (DA)	5 nm/– (200)	[101]
LiNi _{0.7} Co _{0.15} Mn _{0.15} O ₂ / Graphite	1 M Lithium hexafluorophosphate (LiPF ₆) in ethylene carbonate (EC) – ethyl methyl carbonate (EMC)-diethylene carbonate (DEC) (3:4:3, by volume)	0.5 mass% 3-(trimethylsilyl)-2-oxazolidinone (TMS-ON)	3 nm/– (400)	[102]
LiNi _{0.88} Co _{0.09} Al _{0.03} O ₂ / Li	1 M Lithium hexafluorophosphate (LiPF ₆) in ethylene carbonate (EC) -dimethyl carbonate (DMC) (3:7, by volume)	Al ₂ O ₃	200–300 nm/– (300)	[105]
LiNi _{1/3} Co _{1/3} Mn _{1/3} O ₂ / graphite	1 M Lithium hexafluorophosphate (LiPF ₆) – ethylene carbonate (EC)/diethylene carbonate (DEC) (1:3, by mass)	1 mass% Lithium difluorophosphate (LiDFP)	~10 nm/– (100)	[106]
Li _{1.2} Mn _{0.55} Ni _{0.15} Co _{0.1} O ₂ /Li	1 M Lithium hexafluorophosphate (LiPF ₆)-diethylene carbonate (DEC)/ethylene carbonate (EC)/ethyl methyl carbonate (EMC) (2:3:5, by mass)	1 mass% bis(trimethylsilyl)carbodiimide (BTMSC)	6 nm/– (200)	[107]
LiNi _{0.8} Co _{0.15} Al _{0.05} O ₂ / Li	1 M Lithium hexafluorophosphate (LiPF ₆)-diethylene carbonate (DEC)/ethylene carbonate (EC)/ethyl methyl carbonate (EMC) (2:3:5, by mass)	2 mass% N-allyl-N,N-bis(trimethylsilyl)amine (NNB)	10 nm/– (300)	[108]
LiNi _{0.6} Co _{0.2} Mn _{0.2} O ₂ /Li	1 M Lithium hexafluorophosphate (LiPF ₆)-ethylene carbonate (EC)/ethyl methyl carbonate (EMC) (1:2, by mass)	1 mass% 1-(2-cyanoethyl) pyrrole (CEP)	20 nm/– (50)	[109]



Scheme 1. Schematic illustration of nanoengineering of electrode-electrolyte interfaces for advanced Li-ion-based rechargeable batteries.

- 1 The role of the interface and interphase between the electrode and electrolyte will become more critical in the emerging progress from lithium-ion batteries to solid-state lithium batteries.
- 2 Modification in the electrode or electrolyte is the most frequently used method to enhance the interface and interphase between the electrode and electrolyte.
- 3 Instead of adopting only one approach, dual or multiple approaches must simultaneously be taken to improve and optimize the electrode and electrolyte interface.

Different synthetic methods have been employed in the literature to modify the surface of electrode materials. Co-precipitation is usually carried out for surface modification, enabling a thin surface coating.^[32,33] However, its limitations lie in toxic liquid waste and control of pH levels in some cases. Solvothermal/hydrothermal synthesis can employ various solvents, but it also requires an autoclave.^[115] Sol-gel process is a simple method, but it cannot guarantee a uniform coating due to the nature of solution processing. Similar to the sol-gel process, ball-milling is a straightforward method, but it cannot easily control the size of the particle and coating layer.^[116] Atomic layer deposition enables uniform and thin surface coating. Although widely used in the semiconductor industry, it remains a cost-intensive process and might not be scalable in energy storage applications.^[117] UV polymerization is rarely used, but it has the potential to be investigated further. Chemical vapor deposition is useful for the deposition of graphene; However, the processing exhibits similar challenges to atomic layer deposition regarding costs.^[118] Among various used methods for surface modification, atomic layer deposition is most viable for the optimal thickness of the interface since it allows the coating of layers at an atomic scale, as the name indicates. As atomic layer deposition increases production

costs and scalability limitations, alternative methods must also be explored.

In terms of optimal interface composition, electrolyte additive is the most viable approach as the amount of electrolyte additive can lead to the formation of an interphase with a distinct chemical composition, where the amount of electrolyte additive and the chemical composition of the interface are correlated. The goal is to employ a cost-effective and scalable method to form a chemically stable ultrathin interface (<10 nm) with high electric conductivity.

In addition to these points, nanoengineering of the electrode-electrolyte interface and other factors affect the quality of the interphase formed between the electrode and electrolyte. Factors such as applied constant current (or constant voltage) depending on the mass loading of electrode materials and area of the electrode for cycling, formation cycle,^[21] temperature,^[119] and pressure^[120] can also significantly affect the interphase between the electrode and electrolyte. Synergistic technologies are essential to inspect these affecting factors. For example, monitoring gas evolution at the electrode-electrolyte interface, related to unwanted side reactions, can indicate how to

construct the optimal interface. Therefore, differential electrochemical mass spectrometry (DEMS) is a powerful tool for the in-situ detection of gaseous species in rechargeable batteries.^[121,122] Moreover, constant improvement of artificial intelligence (AI, such as ChatGPT) has the potential to systematically evaluate which nanoengineering approach would be optimal for each electrode material in different battery systems and charge/discharge conditions in the future. This will open the door to an exciting path toward advanced energy storage systems that address the growing energy demand.^[119,123]

Acknowledgements

N.-Y.K. and I.K. contributed equally to this work. This work was supported by funding from Bavarian Center for Battery Technology (Baybatt, Hightech Agenda Bayern) and Bayerisch-Tschechische Hochschulagentur (BTHA) (BTHA-AP-2022-45, BTHA-AP-2023-5, and BTHA-AP-2023-12). This work was also supported by the University of Bayreuth-Deakin University Joint Ph.D. Program. This work was also supported by the Regional Innovation Strategy (RIS) through the National Research Foundation of Korea (NRF) funded by the Ministry of Education (MOE) (2021RIS-003). This work was also supported by the National Research Foundation of Korea (NRF) grant funded by the Korea government (MSIT) (No. RS-2023-00213749).

Conflict of Interest

The authors declare no conflict of interest.

Keywords

battery, electrode, electrolyte, interface, lithium, nanoengineering

Received: February 14, 2023
 Revised: March 20, 2023
 Published online: March 23, 2023

- [1] G. E. Blomgren, *J. Electrochem. Soc.* **2017**, *164*, A5019.
- [2] A. Yoshino, *Angew. Chem. Int. Ed.* **2012**, *51*, 5798.
- [3] Y. Wang, B. Liu, Q. Li, S. Cartmell, S. Ferrara, Z. D. Deng, J. Xiao, *J. Power Sources* **2015**, *286*, 330.
- [4] L. Lu, X. Han, J. Li, J. Hua, M. Ouyang, *J. Power Sources* **2013**, *226*, 272.
- [5] J. Duan, X. Tang, H. Dai, Y. Yang, W. Wu, X. Wei, Y. Huang, *Electrochem. Energy Rev.* **2020**, DOI: <https://doi.org/10.1007/s41918-019-00060-4>.
- [6] P. V. Kamat, *ACS Energy Lett.* **2019**, *2019*, 2757.
- [7] H. Wu, G. Chan, J. W. Choi, I. Ryu, Y. Yao, M. T. Mcdowell, S. W. Lee, A. Jackson, Y. Yang, L. Hu, Y. Cui, *Nat. Nanotechnol.* **2012**, *7*, 310.
- [8] J. Chen, X. Fan, Q. Li, H. Yang, M. R. Khoshi, Y. Xu, S. Hwang, L. Chen, X. Ji, C. Yang, H. He, C. Wang, E. Garfunkel, D. Su, O. Borodin, C. Wang, *Nat. Energy* **2020**, *5*, 386.
- [9] N. Ohta, K. Takada, L. Zhang, R. Ma, M. Osada, T. Sasaki, *Adv. Mater.* **2006**, *18*, 2226.
- [10] D. Aurbach, B. Markovsky, G. Salitra, E. Markevich, Y. Talyossef, M. Koltypin, L. Nazar, B. Ellis, D. Kovacheva, *J. Power Sources* **2007**, *165*, 491.
- [11] J. Cabana, B. J. Kwon, L. Hu, *Acc. Chem. Res.* **2018**, *51*, 299.
- [12] X. Yu, A. Manthiram, *Energ. Environ. Sci.* **2018**, *11*, 527.
- [13] H. Yang, J. Lee, J. Y. Cheong, Y. Wang, G. Duan, H. Hou, S. Jiang, I. D. Kim, *Energ. Environ. Sci.* **2021**, *14*, 4228.
- [14] D. Li, H. Guo, S. Jiang, G. Zeng, W. Zhou, Z. Li, *New J. Chem.* **2021**, *45*, 19446.
- [15] J. Yu, S. Liu, G. Duan, H. Fang, H. Hou, *Compos. Commun.* **2020**, *19*, 239.
- [16] H. Bouayad, Z. Wang, N. Dupré, R. Redryvère, D. Foix, S. Franger, J. F. Martin, L. Boutafa, S. Patoux, D. Gonbeau, D. Guyomard, *J. Phys. Chem. C* **2014**, *118*, 4634.
- [17] J. Y. Cheong, J. H. Chang, H. K. Seo, J. M. Yuk, J. W. Shin, J. Y. Lee, I. D. Kim, *Nano Energy* **2016**, *25*, 154.
- [18] X. Yu, A. Manthiram, *Acc. Chem. Res.* **2017**, *50*, 2653.
- [19] Y. Xiao, Y. Wang, S. H. Bo, J. C. Kim, L. J. Miara, G. Ceder, *Nat. Rev. Mater.* **2020**, *5*, 105.
- [20] B. K. Antonopoulos, C. Stock, F. Maglia, H. E. Hoster, *Electrochim. Acta* **2018**, *269*, 331.
- [21] J. Y. Cheong, J. H. Chang, S. H. Cho, J. W. Jung, C. Kim, K. S. Dae, J. M. Yuk, I. D. Kim, *Electrochim. Acta* **2019**, *295*, 7.
- [22] A. Soloy, D. Flahaut, D. Foix, J. Allouche, G. S. Vallverdu, E. Dumont, L. Gal, F. Weill, L. Croguennec, *ACS Appl. Mater. Interfaces* **2022**, *14*, 28792.
- [23] S. T. Myung, K. Amine, Y. K. Sun, *J. Mater. Chem.* **2010**, *20*, 7074.
- [24] S. Kim, W. Cho, X. Zhang, Y. Oshima, J. W. Choi, *Nat. Commun.* **2016**, *7*, 13598.
- [25] X. Ding, D. Luo, J. Cui, H. Xie, Q. Ren, Z. Lin, *Angew. Chem. Int. Ed.* **2020**, *59*, 7778.
- [26] B. J. Kang, J. B. Joo, J. K. Lee, W. Choi, *J. Electroanal. Chem.* **2014**, *728*, 34.
- [27] J. Li, Z. Liu, Y. Wang, R. Wang, *J. Alloys Compd.* **2020**, *834*, 155150.
- [28] J. Song, Y. Wang, Z. Feng, X. Zhang, K. Wang, H. Gu, J. Xie, *ACS Appl. Mater. Interfaces* **2018**, *10*, 27326.
- [29] S. Yang, Q. Fan, Z. Shi, L. Liu, J. Liu, X. Ke, J. Liu, C. Hong, Y. Yang, Z. Guo, *ACS Appl. Mater. Interfaces* **2019**, *11*, 36742.
- [30] S. Deng, X. Li, Z. Ren, W. Li, J. Luo, J. Liang, J. Liang, M. N. Banis, M. Li, Y. Zhao, X. Li, C. Wang, Y. Sun, Q. Sun, R. Li, Y. Hu, H. Huang, L. Zhang, S. Lu, J. Luo, X. Sun, *Energy Storage Mater.* **2020**, *27*, 117.
- [31] Q. Fan, S. Yang, J. Liu, H. Liu, K. Lin, R. Liu, C. Hong, L. Liu, Y. Chen, K. An, P. Liu, Z. Shi, Y. Yang, *J. Power Sources* **2019**, *421*, 91.
- [32] P. Zou, Z. Lin, M. Fan, F. Wang, Y. Liu, X. Xiong, *Appl. Surf. Sci.* **2020**, *504*, 144506.
- [33] W. Zhang, L. Liang, F. Zhao, Y. Liu, L. Hou, C. Yuan, *Electrochim. Acta* **2020**, *340*, 135871.
- [34] M. Wang, Y. Gong, Y. Gu, Y. Chen, L. Chen, H. Shi, *Ceram. Int.* **2019**, *45*, 3177.
- [35] J. Y. Liang, X. X. Zeng, X. D. Zhang, P. F. Wang, J. Y. Ma, Y. X. Yin, X. W. Wu, Y. G. Guo, L. J. Wan, *J. Am. Chem. Soc.* **2018**, *140*, 6767.
- [36] Q. Yang, J. Huang, Y. Li, Y. Wang, J. Qiu, J. Zhang, H. Yu, X. Yu, H. Li, L. Chen, *J. Power Sources* **2018**, *388*, 65.
- [37] Y. Liu, L. Bo Tang, H. Xin Wei, X. Hui Zhang, Z. Jiang He, Y. Jiao Li, J. Chao Zheng, *Nano Energy* **2019**, *65*, 104043.
- [38] X. Wen, K. Liang, L. Tian, K. Shi, J. Zheng, *Electrochim. Acta* **2018**, *260*, 549.
- [39] S. Neudeck, A. Mazilkin, C. Reitz, P. Hartmann, J. Janek, T. Brezesinski, *Sci. Rep.* **2019**, *9*, 5328.
- [40] D. S. Hall, R. Gauthier, A. Eldesoky, V. S. Murray, J. R. Dahn, *ACS Appl. Mater. Interfaces* **2019**, *11*, 14095.
- [41] W. Liu, X. Li, D. Xiong, Y. Hao, J. Li, H. Kou, B. Yan, D. Li, S. Lu, A. Koo, K. Adair, X. Sun, *Nano Energy* **2018**, *44*, 111.
- [42] L. Yao, F. Liang, J. Jin, B. V. R. Chowdari, J. Yang, Z. Wen, *Chem. Eng. J.* **2020**, *389*, 124403.
- [43] X. Li, L. Jin, D. Song, H. Zhang, X. Shi, Z. Wang, L. Zhang, L. Zhu, *J. Energy Chem.* **2020**, *40*, 39.
- [44] D. Becker, M. Börner, R. Nölle, M. Diehl, S. Klein, U. Rodehorst, R. Schmuch, M. Winter, T. Placke, *ACS Appl. Mater. Interfaces* **2019**, *11*, 18404.
- [45] J. C. Zheng, Z. Yang, Z. J. He, H. Tong, W. J. Yu, J. F. Zhang, *Nano Energy* **2018**, *53*, 613.
- [46] C. Zhang, S. Liu, J. Su, C. Chen, M. Liu, X. Chen, J. Wu, T. Huang, A. Yu, *Nanoscale* **2018**, *10*, 8820.
- [47] H. Gao, J. Cai, G. L. Xu, L. Li, Y. Ren, X. Meng, K. Amine, Z. Chen, *Chem. Mater.* **2019**, *31*, 2723.
- [48] Q. Chen, L. Luo, L. Wang, T. Xie, S. Dai, Y. Yang, Y. Li, M. Yuan, *J. Alloys Compd.* **2018**, *735*, 1778.
- [49] Z. Chen, Y. Liu, Z. Lu, R. Hu, J. Cui, H. Xu, Y. Ouyang, Y. Zhang, M. Zhu, *J. Alloys Compd.* **2019**, *803*, 71.
- [50] C. Xu, W. Xiang, Z. Wu, Y. Xu, Y. Li, Y. Wang, Y. Xiao, X. Guo, B. Zhong, *ACS Appl. Mater. Interfaces* **2019**, *11*, 16629.
- [51] T. He, Y. Lu, Y. Su, L. Bao, J. Tan, L. Chen, Q. Zhang, W. Li, S. Chen, F. Wu, *ChemSusChem* **2018**, *11*, 1639.
- [52] C. S. Yoon, U. H. Kim, G. T. Park, S. J. Kim, K. H. Kim, J. Kim, Y. K. Sun, *ACS Energy Lett.* **2018**, *3*, 1634.
- [53] X. Qi, Z. Xue, K. Du, Y. Xie, Y. Cao, W. Li, Z. Peng, G. Hu, *J. Power Sources* **2018**, *397*, 288.
- [54] S. Zhao, B. Sun, K. Yan, J. Zhang, C. Wang, G. Wang, *ACS Appl. Mater. Interfaces* **2018**, *10*, 33260.
- [55] L. Wei, J. Tao, Y. Yang, X. Fan, X. Ran, J. Li, Y. Lin, Z. Huang, *Chem. Eng. J.* **2020**, *384*, 123268.
- [56] W. Xiang, C. Q. Zhu, J. Zhang, H. Shi, Y. T. Liang, M. H. Yu, X. M. Zhu, F. R. He, G. P. Lv, X. D. Guo, *J. Alloys Compd.* **2019**, *786*, 56.
- [57] G. Chen, J. An, Y. Meng, C. Yuan, B. Matthews, F. Dou, L. Shi, Y. Zhou, P. Song, G. Wu, D. Zhang, *Nano Energy* **2019**, *57*, 157.
- [58] K. Liu, Q. Zhang, S. Dai, W. Li, X. Liu, F. Ding, J. Zhang, *ACS Appl. Mater. Interfaces* **2018**, *10*, 34153.
- [59] H. Yang, H. H. Wu, M. Ge, L. Li, Y. Yuan, Q. Yao, J. Chen, L. Xia, J. Zheng, Z. Chen, J. Duan, K. Kisslinger, X. C. Zeng, W. K. Lee, Q. Zhang, J. Lu, *Adv. Funct. Mater.* **2019**, *29*, 1808825.
- [60] Q. Ran, H. Zhao, Y. Hu, S. Hao, Q. Shen, J. Liu, H. Li, Y. Xiao, L. Li, L. Wang, X. Liu, *ACS Appl. Mater. Interfaces* **2020**, *12*, 9268.
- [61] Y. Ma, P. Liu, Q. Xie, G. Zhang, H. Zheng, Y. Cai, Z. Li, L. Wang, Z. Z. Zhu, L. Mai, D. L. Peng, *Nano Energy* **2019**, *59*, 184.

- [62] L. P. Wang, X. D. Zhang, T. S. Wang, Y. X. Yin, J. L. Shi, C. R. Wang, Y. G. Guo, *Adv. Energy Mater.* **2018**, *8*, 1801528.
- [63] G. L. Xu, Q. Liu, K. K. S. Lau, Y. Liu, X. Liu, H. Gao, X. Zhou, M. Zhuang, Y. Ren, J. Li, M. Shao, M. Ouyang, F. Pan, Z. Chen, K. Amine, G. Chen, *Nat. Energy* **2019**, *4*, 484.
- [64] Q. Gan, N. Qin, Y. Zhu, Z. Huang, F. Zhang, S. Gu, J. Xie, K. Zhang, L. Lu, Z. Lu, *ACS Appl. Mater. Interfaces* **2019**, *11*, 12594.
- [65] Y. Cao, X. Qi, K. Hu, Y. Wang, Z. Gan, Y. Li, G. Hu, Z. Peng, K. Du, *ACS Appl. Mater. Interfaces* **2018**, *10*, 18270.
- [66] M. Yoon, Y. Dong, J. Hwang, J. Sung, H. Cha, K. Ahn, Y. Huang, S. J. Kang, J. Li, J. Cho, *Nat. Energy* **2021**, *6*, 362.
- [67] J. Wang, L. Liao, H. R. Lee, F. Shi, W. Huang, J. Zhao, A. Pei, J. Tang, X. Zheng, W. Chen, Y. Cui, *Nano Energy* **2019**, *61*, 404.
- [68] K. R. Tallman, B. Zhang, L. Wang, S. Yan, K. Thompson, X. Tong, J. Thieme, A. Kiss, A. C. Marschilok, K. J. Takeuchi, D. C. Bock, E. S. Takeuchi, *ACS Appl. Mater. Interfaces* **2019**, *11*, 46864.
- [69] S. Heng, X. Shan, W. Wang, Y. Wang, G. Zhu, Q. Qu, H. Zheng, *Carbon* **2020**, *159*, 390.
- [70] D. Jin, J. Park, M. H. Ryou, Y. M. Lee, *Adv. Mater. Interfaces* **2020**, *7*, 1902113.
- [71] L. Wang, L. Zhang, Q. Wang, W. Li, B. Wu, W. Jia, Y. Wang, J. Li, H. Li, *Energy Storage Mater.* **2018**, *10*, 16.
- [72] L. Chen, K. S. Chen, X. Chen, G. Ramirez, Z. Huang, N. R. Geise, H. G. Steinrück, B. L. Fisher, R. Shahbazian-Yassar, M. F. Toney, M. C. Hersam, J. W. Elam, *ACS Appl. Mater. Interfaces* **2018**, *10*, 26972.
- [73] C. Yan, X. B. Cheng, Y. Tian, X. Chen, X. Q. Zhang, W. J. Li, J. Q. Huang, Q. Zhang, *Adv. Mater.* **2018**, *30*, 1707629.
- [74] E. Yi, H. Shen, S. Heywood, J. Alvarado, D. Y. Parkinson, G. Chen, S. W. Sofie, M. M. Doeff, *ACS Appl. Energy Mater.* **2020**, *3*, 170.
- [75] C. Wang, Y. Gong, B. Liu, K. Fu, Y. Yao, E. Hitz, Y. Li, J. Dai, S. Xu, W. Luo, E. D. Wachsman, L. Hu, *Nano Lett.* **2017**, *17*, 565.
- [76] G. V. Alexander, S. Patra, S. V. Sobhan Raj, M. K. Sugumar, M. M. Ud Din, R. Murugan, *J. Power Sources* **2018**, *396*, 764.
- [77] J. Wu, X. Zuo, Q. Chen, X. Deng, H. Liang, T. Zhu, J. Liu, W. Li, J. Nan, *Electrochim. Acta* **2019**, *320*, 134567.
- [78] Z. Zhang, S. Chen, X. Yao, P. Cui, J. Duan, W. Luo, Y. Huang, X. Xu, *Energy Storage Mater.* **2020**, *24*, 714.
- [79] D. Wang, Q. Sun, J. Luo, J. Liang, Y. Sun, R. Li, K. Adair, L. Zhang, R. Yang, S. Lu, H. Huang, X. Sun, *ACS Appl. Mater. Interfaces* **2019**, *11*, 4954.
- [80] F. J. Simon, M. Hanauer, F. H. Richter, J. Janek, *ACS Appl. Mater. Interfaces* **2020**, *12*, 11713.
- [81] J. Zhang, C. Zheng, J. Lou, Y. Xia, C. Liang, H. Huang, Y. Gan, X. Tao, W. Zhang, *J. Power Sources* **2019**, *412*, 78.
- [82] H. Chen, M. X. Jing, C. Han, H. Yang, S. Hua, F. Chen, L. L. Chen, Z. X. Zhou, B. W. Ju, F. Y. Tu, X. Q. Shen, S. B. Qin, *Int. J. Energy Res.* **2019**, *43*, 5912.
- [83] X. Ban, W. Zhang, N. Chen, C. Sun, *J. Phys. Chem. C* **2018**, *122*, 9852.
- [84] H. J. Song, S. H. Jang, J. Ahn, S. H. Oh, T. Yim, *J. Power Sources* **2019**, DOI: <https://doi.org/10.1016/j.jpowsour.2019.01.050>.
- [85] S. H. Jang, K. J. Lee, J. Mun, Y. K. Han, T. Yim, *J. Power Sources* **2019**, *410–411*, 15.
- [86] P. Li, X. Dong, C. Li, J. Liu, Y. Liu, W. Feng, C. Wang, Y. Wang, Y. Xia, *Angew. Chem. Int. Ed.* **2019**, *58*, 2093.
- [87] D. Chen, S. Huang, L. Zhong, S. Wang, M. Xiao, D. Han, Y. Meng, *Adv. Funct. Mater.* **2020**, *30*, 1907717.
- [88] Z. Wang, Y. Wang, Z. Zhang, X. Chen, W. Lie, Y. B. He, Z. Zhou, G. Xia, Z. Guo, *Adv. Funct. Mater.* **2020**, *30*, 2002414.
- [89] Q. Yang, W. Li, C. Dong, Y. Ma, Y. Yin, Q. Wu, Z. Xu, W. Ma, C. Fan, K. Sun, *J. Energy Chem.* **2020**, *42*, 83.
- [90] K. Deng, D. Han, S. Ren, S. Wang, M. Xiao, Y. Meng, *J. Mater. Chem. A* **2019**, *7*, 13113.
- [91] L. Fan, Z. Guo, Y. Zhang, X. Wu, C. Zhao, X. Sun, G. Yang, Y. Feng, N. Zhang, *J. Mater. Chem. A* **2020**, *8*, 251.
- [92] Z. T. Wondimkun, T. T. Beyene, M. A. Weret, N. A. Sahalie, C. J. Huang, B. Thirumalraj, B. A. Jote, D. Wang, W. N. Su, C. H. Wang, G. Brunklaus, M. Winter, B. J. Hwang, *J. Power Sources* **2020**, *450*, 227589.
- [93] P. Zhai, T. Wang, H. Jiang, J. Wan, Y. Wei, L. Wang, W. Liu, Q. Chen, W. Yang, Y. Cui, Y. Gong, *Adv. Mater.* **2021**, *33*, 2006247.
- [94] C. Gao, Q. Dong, G. Zhang, H. Fan, H. Li, B. Hong, Y. Lai, *ChemElectroChem* **2019**, *6*, 1134.
- [95] Q. Ai, Q. Fang, J. Liang, X. Xu, T. Zhai, G. Gao, H. Guo, G. Han, L. Ci, J. Lou, *Nano Energy* **2020**, *72*, 104657.
- [96] Q. Ai, D. Li, J. Guo, G. Hou, Q. Sun, X. Xu, W. Zhai, L. Zhang, J. Feng, P. Si, J. Lou, L. Ci, *Adv. Mater. Interfaces* **2019**, *6*, 1901187.
- [97] S. G. Patnaik, T. P. Jayakumar, Y. Sawamura, N. Matsumi, *ACS Appl. Energy Mater.* **2021**, *4*, 2241.
- [98] J. Guo, W. Wu, J. Wang, T. Zhang, R. Wang, D. Xu, C. Wang, Y. Deng, *Solid State Ion.* **2020**, *347*, 115272.
- [99] X. Zhang, L. Zou, Y. Xu, X. Cao, M. H. Engelhard, B. E. Matthews, L. Zhong, H. Wu, H. Jia, X. Ren, P. Gao, Z. Chen, Y. Qin, C. Kompella, B. W. Arey, J. Li, D. Wang, C. Wang, J. G. Zhang, W. Xu, *Adv. Energy Mater.* **2020**, *10*, 202000368.
- [100] J. B. Goodenough, Y. Kim, *Chem. Mater.* **2010**, *22*, 587.
- [101] F. Cheng, X. Zhang, Y. Qiu, J. Zhang, Y. Liu, P. Wei, M. Ou, S. Sun, Y. Xu, Q. Li, C. Fang, J. Han, Y. Huang, *Nano Energy* **2021**, *88*, 106301.
- [102] K. Kim, D. Hwang, S. Kim, S. O. Park, H. Cha, Y. S. Lee, J. Cho, S. K. Kwak, N. S. Choi, *Adv. Energy Mater.* **2020**, *10*, 2000012.
- [103] J. C. Burns, N. N. Sinha, G. Jain, H. Ye, C. M. VanElzen, E. Scott, A. Xiao, W. M. Lamanna, J. R. Dahn, *J. Electrochem. Soc.* **2013**, *160*, A2281.
- [104] D. J. Xiong, R. Petibon, L. Madec, D. S. Hall, J. R. Dahn, *J. Electrochem. Soc.* **2016**, *163*, A1678.
- [105] Y. Y. Sun, S. Liu, Y. K. Hou, G. R. Li, X. P. Gao, *J. Power Sources* **2019**, *410–411*, 115.
- [106] C. Wang, L. Yu, W. Fan, J. Liu, L. Ouyang, L. Yang, M. Zhu, *ACS Appl. Energy Mater.* **2018**, *1*, 2647.
- [107] J. Lan, Q. Zheng, H. Zhou, J. Li, L. Xing, K. Xu, W. Fan, L. Yu, W. Li, *ACS Appl. Mater. Interfaces* **2019**, *11*, 28841.
- [108] Q. Zheng, L. Xing, X. Yang, X. Li, C. Ye, K. Wang, Q. Huang, W. Li, *ACS Appl. Mater. Interfaces* **2018**, *10*, 16843.
- [109] B. Liao, X. Hu, M. Xu, H. Li, L. Yu, W. Fan, L. Xing, Y. Liao, W. Li, *J. Phys. Chem. Lett.* **2018**, *9*, 3434.
- [110] R. S. Arumugam, L. Ma, J. Li, X. Xia, J. M. Paulsen, J. R. Dahn, *J. Electrochem. Soc.* **2016**, *163*, A2531.
- [111] Y. Zhao, J. Li, J. R. Dahn, *Chem. Mater.* **2017**, *29*, 5239.
- [112] F. Wang, Y. Lin, L. Suo, X. Fan, T. Gao, C. Yang, F. Han, Y. Qi, K. Xu, C. Wang, *Energy Environ. Sci.* **2016**, *9*, 3666.
- [113] H. Chen, J. Chen, W. Zhang, Q. Xie, Y. Che, H. Wang, L. Xing, K. Xu, W. Li, *J. Mater. Chem. A* **2020**, *8*, 22054.
- [114] S. Tan, Z. Shadike, J. Li, X. Wang, Y. Yang, R. Lin, A. Cresce, J. Hu, A. Hunt, I. Waluyo, L. Ma, F. Monaco, P. Cloetens, J. Xiao, Y. Liu, X.-Q. Yang, K. Xu, E. Hu, *Nat. Energy* **2022**, *7*, 484.
- [115] V. K. Suhas, L. P. Gupta, M. Singh, S. K. Chaudhary, *J. Clean. Prod.* **2021**, *288*, 125643.
- [116] R. M. Raihanuzzaman, T. S. Jeong, R. Ghomashchi, Z. Xie, S. J. Hong, *J. Alloys Compd.* **2014**, *615*, S564.
- [117] A. Karimghaloo, J. Koo, H. Sen Kang, S. A. Song, J. H. Shim, M. H. Lee, *Int. J. Precis. Eng. Manuf. Green Technol.* **2019**, *6*, 611.
- [118] Y. Hamedani, P. Macha, T. J. Bunning, R. R. Naik, M. C. Vasudev, *Plasma-Enhanced Chemical Vapor Deposition: Where we are and the Outlook for the Future*, InTech, **2016**. https://books.google.de/books?hl=ko&lr=&id=k3eQDwAAQBAJ&oi=fnd&pg=PA247&dq=Plasma-Enhanced+Chemical+Vapor+Deposition:+Where+We+are+and+the+Outlook+for+the+Future&ots=DiBKOe8Vy&sig=_9wil6W59N8rGbMrYB-M1v2Tf2w&redir_esc=y#v=onepage&q=Plasma-Enhanced%20Chemical%20Vapor%20Deposition%3A%20Where%20We%20are%20and%20the%20Outlook%20for%20the%20Future&f=false (accessed: April 2023).

- [119] A. Maraschky, R. Akolkar, *J. Electrochem. Soc.* **2020**, *167*, 62503.
- [120] R. M. Kasse, N. R. Geise, E. Sebti, K. Lim, C. J. Takacs, C. Cao, H. G. Steinrück, M. F. Toney, *ACS Appl. Energy Mater.* **2022**, *5*, 8273.
- [121] S. J. Davis, N. S. Lewis, M. Shaner, S. Aggarwal, D. Arent, I. L. Azevedo, S. M. Benson, T. Bradley, J. Brouwer, Y. M. Chiang, C. T. M. Clack, A. Cohen, S. Doig, J. Edmonds, P. Fennell, C. B. Field, B. Hannegan, B. M. Hodge, M. I. Hoffert, E. Ingersoll, P. Jaramillo, K. S. Lackner, K. J. Mach, M. Mastrandrea, J. Ogden, P. F. Peterson, D. L. Sanchez, D. Sperling, J. Stagner, J. E. Trancik, C. J. Yang, K. Caldeira, *Science* **2018**, *360*, eaas9793.
- [122] M. Fichtner, K. Edström, E. Ayerbe, M. Berecibar, A. Bhowmik, I. E. Castelli, S. Clark, R. Dominko, M. Erakca, A. A. Franco, A. Grimaud, B. Horstmann, A. Latz, H. Lorrman, M. Meeus, R. Narayan, F. Pammer, J. Ruhland, H. Stein, T. Vegge, M. Weil, *Adv. Energy Mater.* **2022**, *12*, 2102904.
- [123] Q. Wang, L. Velasco, B. Breitung, V. Presser, *Adv. Energy Mater.* **2021**, *11*, 2102355.